Polymer 51 (2010) 2013–2020

Contents lists available at ScienceDirect

Polymer

journal homepage: www.elsevier.com/locate/polymer

Analysis and modeling of the mechanical properties of novel thermotropic polymer biomaterials

C.S. Lovell [a], H. Montes de Oca [b], D. Farrar [b], M.E. Ries [a], I.M. Ward [a,*]

[a] School of Physics & Astronomy, University of Leeds, Leeds LS2 9JT, United Kingdom
[b] Smith & Nephew Research Centre, York Science Park, Heslington York YO10 5DF, United Kingdom

ARTICLE INFO

Article history:
Received 14 January 2010
Received in revised form
23 February 2010
Accepted 26 February 2010
Available online 6 March 2010

Keywords:
Biomaterial
Liquid crystalline polymers
Aggregate model

ABSTRACT

A series of random aromatic-aliphatic thermotropic copolyesters comprising *p*-hydroxybenzoic acid (HBA), vanillic acid (VA), 4,4′-sulfonyl *bis*(2-methylphenol) (dBPS) and three aliphatic diacids (Spacer), developed for potential applications in orthopaedic medicine, have been characterized in the context of their structure and mechanical properties. Each of the three polymers comprised the following molar percentages of monomer units 50/25/12.5/12.5 (HBA/VA/dBPS/Spacer). Oriented fibres prepared from the materials via melt-spinning have been analyzed using X-ray diffraction to evaluate order parameters describing the degree of molecular orientation and mechanical measurements to determine their tensile properties. In addition, measurements of the bulk isotropic and shear moduli of one polymer composition have also been performed. To obtain an understanding of the material properties the aggregate model due to Ward has been applied to the orientation dependence of the measured elastic moduli and the development of mechanical anisotropy.

1. Introduction

Polyesters derived from glycolic acid and lactic acid are examples of bioresorbable polymers used extensively in orthopaedic medicine as rods, plates, pins and screws to provide mechanical support to fractured bone-tissue during the healing process [1,2]. Recently the structure and properties of oriented poly(glycolic acid) [3–5] and poly(L-lactic acid) [6] fibres have been investigated with the aim of developing bioresorbable materials to address the physiological requirements for high load-bearing orthopaedic applications, for example the fixation of cortical bone-tissue, which currently necessitate the use of metallic implants. The tensile stiffness and strength of cortical bone are reported to range 7–25 GPa and 50–160 MPa respectively [7]. However, these materials have been found not to provide a suitable combination of mechanical performance and resorption properties to practically resolve the issue of providing long-term tissue support during the healing process. In this regard there is a need for novel bioresorbable materials which may be fabricated into devices to provide a suitable alternative to conventional therapies in fracture fixation. During the last decade the synthesis of bioresorbable liquid crystalline polymers (LCPs) has received attention from several groups as a potential solution [8–14].

In materials science liquid crystalline aromatic polyamides and polyesters are recognized for their excellent mechanical properties when processed into highly oriented fibres and tapes [15–17]. However, commercially available liquid crystalline materials are not bioresorbable. Research efforts have therefore focused on the synthesis of novel thermotropic liquid crystalline polymers comprised of moieties which will allow the polymer to degrade through hydrolysis under physiological conditions. Degradative properties are achieved through the incorporation of aliphatic carboxyl groups [8], whilst the mesogenic character is encouraged through the incorporation of extended sequences of aromatic units. It is important to recognize for medical applications the choice of suitable aromatic moieties is restricted primarily due to their toxicity.

This paper concerns the characterization of new polymeric liquid crystalline biomaterials developed by Smith & Nephew® and an analysis of the structure and mechanical properties of the materials.

2. Experimental

2.1. Materials

Copolyesters derived from the random synthesis of *p*-hydroxybenzoic acid (HBA), vanillic acid (VA), 4,4′-sulfonyl *bis*(2-methylphenol) (dBPS) and each of the following aliphatic diacids (Spacer),

* Corresponding author.
E-mail addresses: cs.lovell@me.com (C.S. Lovell), horacio.montesdeoca@smith-nephew.com (H. Montes de Oca), david.farrar@smith-nephew.com (D. Farrar), m.e.ries@leeds.ac.uk (M.E. Ries), i.m.ward@leeds.ac.uk (I.M. Ward).

0032-3861/$ – see front matter © 2010 Elsevier Ltd. All rights reserved.
doi:10.1016/j.polymer.2010.02.047

adipic acid (AD), suberic acid (SUB) and azelaic acid (AZ), were prepared at the University of York by Dr. A.D. Wilson; details of the polymer synthesis, hydrolytic degradation and biocompatibility of these materials are to be presented in separate publication by Montes de Oca et al. [18]. It is noted from a structural perspective that the polymer composition addresses each of the established aspects of LCP design required to frustrate crystallization and improve melt-processability, that is, the incorporation of flexible spacer units, rigid-kinked units and substituent side-groups, and a random synthesis of comonomers [19]. Optical observations have confirmed that each of the compositions forms a stable nematic mesophase.

The polymers investigated in this work were synthesized with the same ratio of component monomers 50/25/12.5/12.5 (HBA/VA/dBPS/Spacer). In the following discussion the three materials will be referred to as 75-AD, 75-SUB and 75-AZ reflecting the combined HBA and VA content of 75 mol% and the respective aliphatic diacid used in each of the three compositions. Details of the polymer molecular weights listed in Table 1 were provided by Smith & Nephew® (measured by gel permeation chromotography relative to poly(styrene) standards).

2.2. Processing

Facilities at the University of Leeds and Smith & Nephew Research Centre were used to prepare fibres via melt-extrusion through a capillary die and subsequent draw-down of the extruded monofilament using a haul-off unit. In each set-up a heated extruder barrel and die was attached to a supporting frame mounted within an Instron. Controlled extrusion of the polymer melt was achieved using a computer to set and regulate the speed of a ram plunger which was secured to the Instron cross-head arm. Initially the raw polymer powders were introduced to the heated barrel at 180 °C and compacted at temperature to produce well consolidated billets of material prior to extrusion. The temperature of the barrel and die was then increased to an appropriate extrusion temperature for melt-spinning fibres. The processing conditions for each of the materials are listed in Table 2.

Test specimens for dynamic mechanical measurements were prepared by compression moulding materials at 160 °C; for this purpose a rectangular steel mould was used to produce bars with dimensions 1.23 ± 0.01 mm × 5.10 ± 0.02 mm × 50 mm.

2.3. Tensile measurements

Fibre tensile stress-strain behaviours were evaluated using an Instron 5500. A fibre gauge length of 50 mm and an extensional rate of 5 mm min^{-1} was employed in all tests. A digital micrometer was used to take measurements of fibre diameters and the mean fibre cross-sectional area was calculated from the average fibre diameter evaluated along the length of the test specimen.

2.4. Dynamic measurements

A Rheometrics RDA II Rheometer was used to perform measurements of the bulk dynamic shear modulus using a rectangular torsional geometry. Values of the dynamic shear modulus calculated from the angular deformation and corresponding torque measurement were corrected following St Venant [16,20]. The corresponding isotropic elastic modulus was measured using a Rheometrics RSA II Solids Analyzer employing a three point bending geometry. Room temperature dynamic measurements in both torsion and bending were performed at 1 rad s^{-1}.

Table 1
Polymer molecular weights.

Material	$\overline{M}_n$	$\overline{M}_w$
75-AD	13700	24800
75-SUB	16500	32200
75-AZ	16000	33500

Table 2
Fibre processing conditions.

Fibre	Die capillary aspect ratio	Die temperature/°C	Extrusion rate/m min^{-1}	Haul-off rate/m min^{-1}
75-AD(225)	6	225	0.50	44
75-AD(205)	6	205	0.50	44
75-SUB	6	235	0.15	35
75-AZ	2	232	0.22	25

2.5. Wide-angle X-ray diffraction

Textural measurements of the fibre wide-angle X-ray diffraction (WAXD) patterns were performed using a laboratory Hiltonbrooks X-ray generator and Huber Texture Goniometer 4020. A Huber 9900 scintillation counter was used to measure the intensity of Cu-K_α radiation. All experiments were performed using the symmetric transmission geometry for which samples were prepared in small fibre bundles. The fibre equatorial and meridional scattering profiles were measured in 2θ across the angular range from 10.0° to 50.0°. In performing orientation measurements on fibres 2θ was fixed at 20.0° (equatorial peak position) and the angle χ between the fibre axis and the vertical of the goniometer was incremented over the angular range from 90° to 270°.

3. Results

3.1. Mechanical properties

Measurements of the fibre true stress–strain behaviour for 75-AD, 75-SUB and 75-AZ are shown in Fig. 1. The results presented correspond to tests displaying the maximum observed true-strain at break. An inspection of the stress–strain behaviour highlights features which are typical for extensional deformations of amorphous polymer glasses, that is, an elastic regime extending over

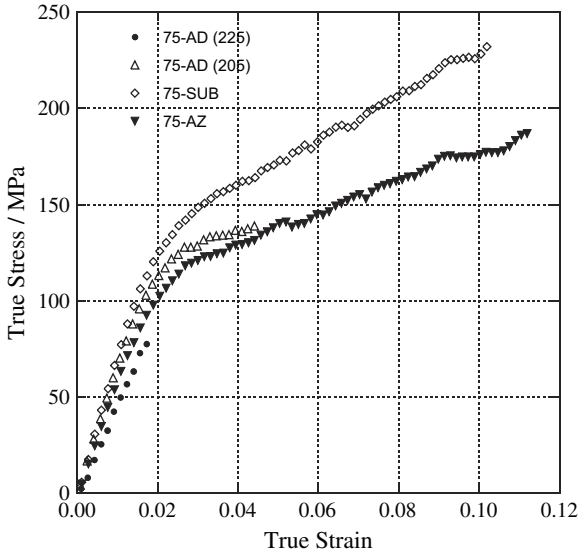

Fig. 1. Measurements of the fibre true stress–strain behaviour for 75-AD fibres processed at 205 °C and 225 °C, 75-SUB and 75-AZ fibres.

small strains (i.e., $\varepsilon < 0.02$), a yield point and brittle failure [16,21]. Inconsistencies in the brittle failure of the test specimens noted in additional tests presumably reflected differences in the extent and nature of structural defects within the fibres. Molecular weight is also known to influence the tensile strength of materials and may explain the failure of 75-AD fibres at lower strain values than 75-SUB and 75-AZ materials.

In Table 3 properties evaluated from the tensile tests are recorded for each of the polymer compositions, specifically, the fibre moduli, the fibre strengths, strain-at-break and the yield stresses and strains. The fibre moduli were determined using data points at small strains, $\varepsilon \leq 0.01$. The yield stresses and yield strains were evaluated from the point of intersection between tangents drawn to the initial and final regions of the stress–strain curves. Values reported in Table 3 for the fibre moduli and yield stresses are averages obtained from five repeated tests.

Although several research groups have worked on the synthesis and degradative properties of bioresorbable liquid crystalline polymers few details of the mechanical performance of these materials have been published. In their work on degradable thermotropic copolyesters with lactide moieties Haderlein et al. [10] report a value of 6–8 GPa for the tensile moduli of monofilaments drawn from the melt. The fibre tensile properties achieved in this present work are also comparable to properties reported by Blumstein et al. [22] in their work on a series of regularly sequenced aromatic–aliphatic LCPs; the maximum fibre tensile modulus and strength reported were 7.7 GPa and 240 MPa.

The isotropic properties of the 75-AD polymer composition measured at room temperature using dynamic mechanical three-point bending and torsional tests are given in Table 4.

3.2. Wide-angle X-ray diffraction patterns

The WAXD patterns obtained from 75-AD, 75-SUB and 75-AZ fibres were found to display equatorial and meridional scattering features characteristic of a nematic chain registry. A photograph of WAXD pattern obtained 75-SUB fibres is presented in Fig. 2(a). The broad scattering profile corresponding to the azimuthal variation of the equatorial scattering intensity dominates the WAXD pattern and is qualitatively indicative of low molecular orientation. Two diffuse meridional scattering features are visible along the vertical of the photograph. Quantitative measurements taken using the Huber goniometer established that the positions of the equatorial and meridional scattering peaks in 2θ were indistinguishable reflecting both the chemical and structural similarities of the three polymer compositions. These results are presented in Fig. 2(b) and (c) respectively.

The lateral organisation of the chains is clearly disordered as evidenced by the breadth of the equatorial scattering peak, in this sense the materials are amorphous. The amorphous morphology presumably reflects an intrinsic level of disorder relating to the polymer composition.

Nematic order is inferred from the meridional scattering interferences. Blackwell and co-workers have extensively studied WAXD meridional scattering patterns obtained from oriented LCPs and established that the peaks correspond to intrachain coherences resulting from extended chain conformations within the nematic domains [23–26]. In Fig. 2(c) the broad scattering upon which the meridional scattering is superposed corresponds to interchain scattering from domains oriented perpendicular to the fibre axis. Correspondingly very weak scattering is observed at $2\theta = 44.0^\circ$ in Fig. 2(b) due to intrachain coherences within these same domains.

Studies on several wholly aromatic LCPs have demonstrated that the polymer chains can adopt very efficient lateral packing arrangements, yielding sharp equatorials and off-equatorial scattering peaks indicative of three-dimensional order [19,26]. Further, improvements in the lateral registry of the polymer chains within these materials have been reported following annealing treatments resulting in improved tensile properties [27]. Annealing fibres prepared in this work at temperatures above their glass-transition temperature ($T_g \approx 100\ ^\circ C$) resulted in substantial shrinkage and, therefore, the treatment was detrimental to their mechanical performance.

Table 3
Tensile properties of oriented fibres.

Fibre	Modulus/GPa	Strength (max.)/MPa	Strain-at-break (max.)/MPa	Yield stress/MPa	Yield strain/%
75-AD(225)	4.7 ± 0.3	80 ± 10	1.8	–	–
75-AD(205)	6.2 ± 0.3	140 ± 20	4.5	120 ± 10	1.9
75-SUB	7.6 ± 0.1	230 ± 20	10.2	138 ± 5	1.8
75-AZ	5.9 ± 0.1	190 ± 20	11.2	107 ± 5	1.8

Table 4
Properties of an isotropic material measured in dynamic mechanical tests at 1 rad s^{-1}.

Material	Elastic modulus/GPa	Shear modulus/GPa
75-AD	3.3 ± 0.2	1.2 ± 0.1

3.2.1. Order parameters

Methods described by Mitchell and Windle [28–30] for the analysis of the azimuthal dependence of the scattering intensity of the fibre equatorials were used to evaluate orientation parameters. To summarize, the experimentally observed azimuthal scattering intensity of the fibre equatorial, $I(q, \alpha)$, is considered to result from the convolution of the scattering intensity from a perfectly ordered domain, $I_m(q, \beta)$, and a distribution of domain orientations, $D(\psi)$:

$$I(q,\alpha) = I_m(q,\beta) * D(\psi). \quad (1)$$

In Equation (1) the variables are defined as follows: q is the scattering vector, α is the angle between the fibre axis and the normal to the observed scattering planes, β is the angle between the laboratory axis (i.e., the goniometer vertical) and the principal axis of a domain and ψ is the angle between the fibre axis and the principal axis of a domain. The convolution of orientation distributions is illustrated in Fig. 3.

Given the assumption of cylindrical symmetry each of the distributions, $I(q, \alpha)$, $I_m(q, \beta)$ and $D(\psi)$ may be expanded in terms of a spherical harmonic series of even-order, for example

$$I(q,\alpha) = \sum_{n=0}^{\infty} I_{2n}(q) P_{2n}(\cos\alpha), \quad (2)$$

where $I_{2n}(q)$ are the coefficients of the spherical harmonic expansion. Similarly, $I_m(q, \beta)$ and $D(\psi)$ are expanded in the same manner. Deas [31] evaluated the convolution given by Equation (1) and derived a relationship between the coefficients of each harmonic series. The result is conveniently expressed by Mitchell and Windle [29,30]:

$$\langle P_{2n}(\cos\alpha)\rangle = \langle P_{2n}(\cos\alpha)\rangle_m \langle P_{2n}(\cos\psi)\rangle_d \quad (3)$$

where $\langle P_{2n}(\cos\alpha)\rangle$ are the order parameters evaluated from the azimuthal scattering intensity of the fibre equatorials, $\langle P_{2n}(\cos\alpha)\rangle_m$ are order parameters describing the perfectly ordered domain and $\langle P_{2n}(\cos\psi)\rangle_d$ are the order parameters describing the distribution of domain orientations.

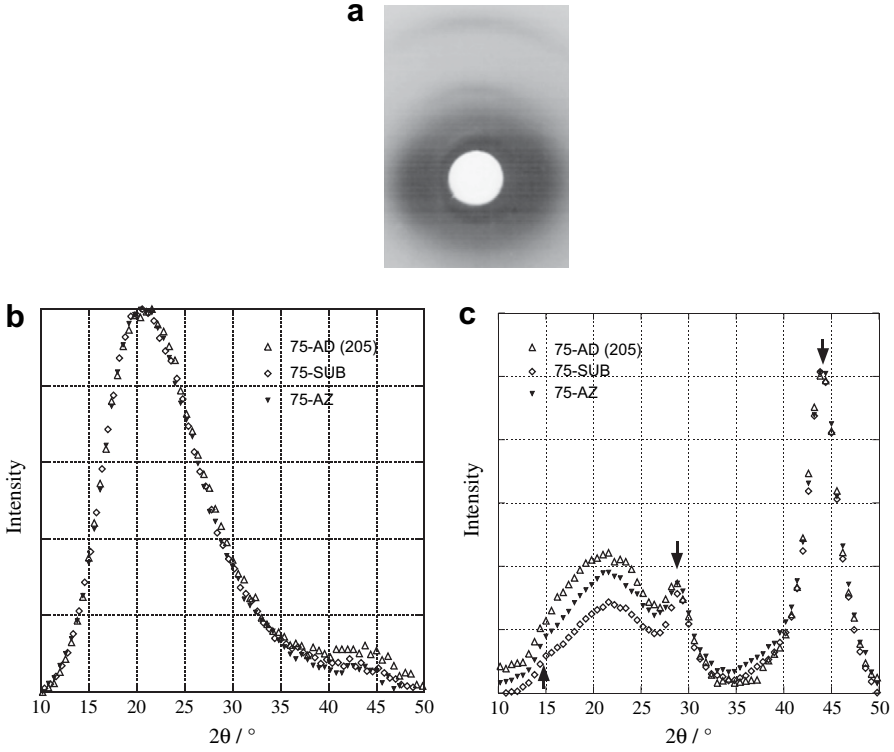

Fig. 2. (a) A photograph of 75-SUB fibre WAXD pattern characteristic of nematic chain registry. Comparisons of (b) equatorial and (c) meridional scattering profiles obtained from 75-AD fibres processed at 205 °C, 75-SUB and 75-AZ fibres which demonstrate the structural similarities of the materials.

The degree of molecular orientation within the fibres has been quantified by evaluating the order parameters

$$\langle P_2(\cos\alpha)\rangle = \frac{1}{2}\left(3\left\langle\cos^2\alpha\right\rangle - 1\right) \tag{4}$$

and

$$\langle P_4(\cos\alpha)\rangle = \frac{1}{8}\left(35\left\langle\cos^4\alpha\right\rangle - 30\left\langle\cos^2\alpha\right\rangle + 3\right). \tag{5}$$

from experimental measurements of the scattering intensity. The order parameters describing the perfectly ordered domain are given by

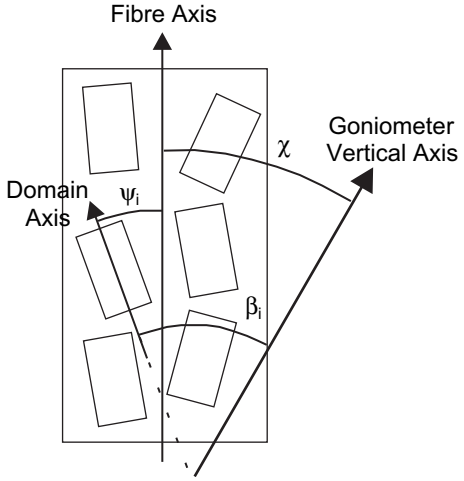

Fig. 3. The diagram illustrates the convolution of orientation distributions for uniaxial symmetry.

$$\langle P_{2n}(\cos\alpha)\rangle_m = \frac{(2n!)}{(-1)^n 2^{2n}(n!)^2}. \tag{6}$$

Table 5 lists the values for domain order parameters $\langle P_2(\cos\psi)\rangle_d$ and $\langle P_4(\cos\psi)\rangle_d$ obtained using Equation (3). Uncertainties in the values are calculated based on an estimated 10% uncertainty in the absolute value of the background scattering intensity at $2\theta = 20.0^{\circ}$ for each of the samples.

The values obtained for the order parameters emphasize the low levels of molecular orientation developed during fibre processing and provide a justification for the relatively low values obtained for the fibre tensile moduli in comparison with high modulus and high strength wholly aromatic LCP fibres which are characterized by a very high degree of molecular orientation, where typically $\langle P_2(\cos\alpha)\rangle_d > 0.95$.

3.2.2. Orientation distributions

A general observation has been made in studies on uniaxially oriented polymers that the molecular orientation distribution is reasonably described by the distribution of maximum entropy [32],

$$D_{s_{\max}}(\alpha) = \exp\sum_n a_{2n}P_{2n}(\cos\alpha), \tag{7}$$

where a_{2n} are Lagrange multipliers, $P_{2n}(\cos\alpha)$ are the spherical harmonics and the sum is taken over number of known order

Table 5
Order parameters for the domain orientation distributions.

Fibre	$\langle P_2(\cos\psi)\rangle_d$	$\langle P_4(\cos\psi)\rangle_d$
75-AD(225)	0.20 ± 0.01	0.034 ± 0.001
75-AD(205)	0.46 ± 0.04	0.18 ± 0.02
75-SUB	0.51 ± 0.06	0.21 ± 0.03
75-AZ	0.46 ± 0.02	0.18 ± 0.01

parameters determined from experiment (i.e., $n = 0$, 1 and 2). To determine the profile of the distribution of maximum entropy a least-squares regression of the values for the Lagrange multipliers, a_0, a_2 and a_4, was performed given the following series of constraints,

$$\frac{\int_0^{\pi/2} P_{2n}(\cos\alpha) D_{s_{max}}(\alpha) \sin\alpha \, d\alpha}{\int_0^{\pi/2} D_{s_{max}}(\alpha) \sin\alpha \, d\alpha} = \langle P_{2n}(\cos\alpha)\rangle, \quad (8)$$

where $\langle P_{2n}(\cos\alpha)\rangle$ take values determined from experimental measurements.

In Fig. 4 a comparison is drawn between the experimental azimuthal dependence of the scattering intensity measured for 75-AD, 75-SUB and 75-AZ fibres and the corresponding distributions of maximum entropy which yield equivalent values for the order parameters $\langle P_2(\cos\alpha)\rangle$ and $\langle P_4(\cos\alpha)\rangle$. The result demonstrates molecular orientation is well described by the distribution of maximum entropy.

4. Discussion

The aim of this work has been to understand the mechanical properties of the materials in terms of their structure and the development of molecular orientation. Although the materials have been processed under different conditions and on different systems WAXD studies have demonstrated that the morphologies of the resulting fibres are indistinguishable. A generic analysis of the elastic material properties has therefore been constructed in the context of the aggregate model due to Ward [16,33] using measurements of the elastic moduli of oriented fibres, the evaluation of orientation parameters from the fibre WAXD patterns and measurements of the isotropic elastic and shear moduli of an unoriented sample.

The aggregate model is valid for single-phase polymer systems and has been used extensively to describe the mechanical anisotropy of oriented amorphous, low-crystallinity and liquid crystalline polymer materials [16]. In applying the model the bulk material properties are taken as the average over an aggregate of identical subunits weighted by an orientation distribution. The development of bulk mechanical anisotropy is considered to result purely from a geometric rearrangement of the constituent subunits during the orientation process.

The aggregate model therefore provides a suitable framework which analyzes the material properties.

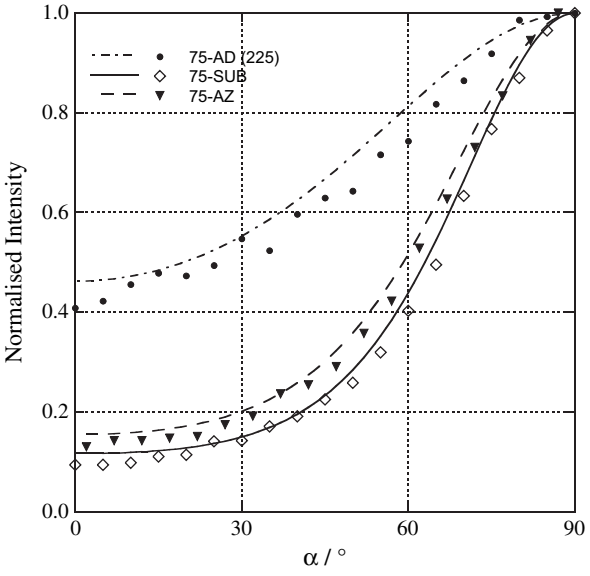

Fig. 4. A comparison of calculated maximum entropy distributions and experimental measurements of the azimuthal dependence of fibre equatorial scattering intensity.

4.1. Aggregate modeling

In modeling the properties of oriented LCPs the assumption of uniform stress (i.e., a Reuss average) has proved an applicable scheme [16]. Making the simplifying assumptions of both orthorhombic symmetry and transverse symmetry in the plane perpendicular to the primary axis the properties of the aggregate may then be related to five independent elastic constants describing the subunit properties. Under the scheme of the Reuss average the axial compliance of the aggregate is given by Equation (9):

$$s'_{33} = s_{11}\left\langle \sin^4\psi \right\rangle + s_{33}\left\langle \cos^4\psi \right\rangle + \langle 2s_{13} + s_{44}\rangle \left\langle \sin^2\psi \cos^2\psi \right\rangle \quad (9)$$

where s'_{33} is the axial compliance of the aggregate, s_{33} is the axial compliance of the subunit, s_{11} is the transverse compliance of the subunit, s_{44} is the shear compliance of the subunit and terms in chevron brackets represent averages of the cosines and sines taken over the aggregate orientation distribution. The term s_{13} is given by

$$s_{13} = -\nu_{13} s_{33} \quad (10)$$

where ν_{13} is the Poisson's ratio. In previous work on highly oriented fibres and tapes the subunit has been assumed to correspond to a nematic structural unit with dimensions equivalent to each of the scattering lengths yielding the meridional and equatorial scattering in WAXD experiments. In such examples the structural subunit has been shown to possess a large mechanical anisotropy, where $s_{44} > s_{11} \gg s_{33}$, due to the extended conformation of highly oriented polymer chains [27,34–36]. The axial compliance of the aggregate was successfully modeled in terms of the axial and shear compliances of the subunit:

$$s'_{33} \approx s_{33} + s_{44}\left\langle \sin^2\psi \right\rangle \quad (11)$$

where the respective compliances are considered to be equivalent to the reciprocal of the experimental values of the fibre modulus, X-ray crystal modulus and bulk shear modulus ($s'_{33} = 1/E_f$, $s_{33} = 1/E_c$ and $s_{44} = 1/G$ respectively).

Due to the low molecular orientation evident from X-ray measurements for the fibres studied in this work it is important to retain all terms within the aggregate model. To provide an instructive analysis of the material properties with the available information the axial compliance of the aggregate (see Equation (9)) was considered in the following form,

$$s'_{33} = s_{11} + (s_{33} - s_{11})\left\langle \cos^2\psi \right\rangle + (s_{44} - s_{11} - (1 + 2\,\nu_{13})s_{33}) \times \left\langle \sin^2\psi \cos^2\psi \right\rangle, \quad (12)$$

where substitutions have been made for the orientation averages $\langle \sin^4\psi\rangle$ and $\langle \cos^4\psi\rangle$ using relationships given in the Appendix. An analysis may now be conducted with regard to the orientation dependence of the fibre moduli using Equation 12 which defines the axial compliance in terms of the orientation averages $\langle \cos^2\psi\rangle$ and $\langle \sin^2\psi \cos^2\psi\rangle$.

In Fig. 5 the reciprocal of both the fibre moduli and the isotropic bulk modulus of the unoriented bar are plotted against the orientation average $\langle\cos^2\psi\rangle$. It is evident from the experimental data that there is an approximately linear dependence of the fibre compliance on the orientation average $\langle\cos^2\psi\rangle$. Inspecting the aggregate model description given by Equation 12 this result implies that the subunit axial and transverse compliances, s_{11} and s_{44}, are approximately equal (i.e., the term associated with $\langle\sin^2\psi\cos^2\psi\rangle$ is then much smaller than the term associated with $\langle\cos^2\psi\rangle$). Equation 12 can then be reduced to the linear expression,

$$s'_{33} \approx s_{11} + (s_{33} - s_{11})\left\langle\cos^2\psi\right\rangle. \tag{13}$$

Considering that the aggregate subunit will have a finite axial compliance, s_{33} has been defined to take a value of 0.01 GPa^{-1}. This is consistent with experimental measurements of the crystal chain modulus of wholly aromatic LCPs [27,34–36]. By fitting Equation 13 to the experimental data the above considerations yield the following common value for the transverse and shear compliances of the aggregate subunit, $s_{11} = s_{44} = 0.43 \pm 0.01$ GPa^{-1}.

Further analysis is also presented in Fig. 5 assuming each of the following relationships between the subunit shear and transverse compliances: $s_{44} = 3/2\ s_{11}$, $s_{44} = 2\ s_{11}$ and $s_{44} = 3\ s_{11}$. For the stated cases, it can be seen that the term associated with $\langle\sin^2\psi\cos^2\psi\rangle$ in Equation 12 is now significant. To apply the aggregate model it was necessary, however, to first address the relationship between the orientation averages $\langle\cos^2\psi\rangle$, $\langle\sin^2\psi\cos^2\psi\rangle$ and $\langle\cos^4\psi\rangle$.

To explain, consider that the distribution of maximum entropy was found to provide a reasonable description of molecular orientation within the fibres and it was noted this has been a general observation in studies of uniaxially oriented polymers. To illustrate the generic relationship between orientation averages $\langle\cos^2\psi\rangle$ and $\langle\cos^4\psi\rangle$ for uniaxially oriented polymers the results obtained in this work and in works originally published by Unwin et al. [37] on studies of oriented poly(propylene) and Mitchell and Windle [29] on oriented poly(hydroxybenzoic acid-co-ethylene terephthalate) are presented in Fig. 6. The relationship between $\langle\cos^2\psi\rangle$ and $\langle\cos^4\psi\rangle$ has been defined in terms of a polynomial expansion of the form,

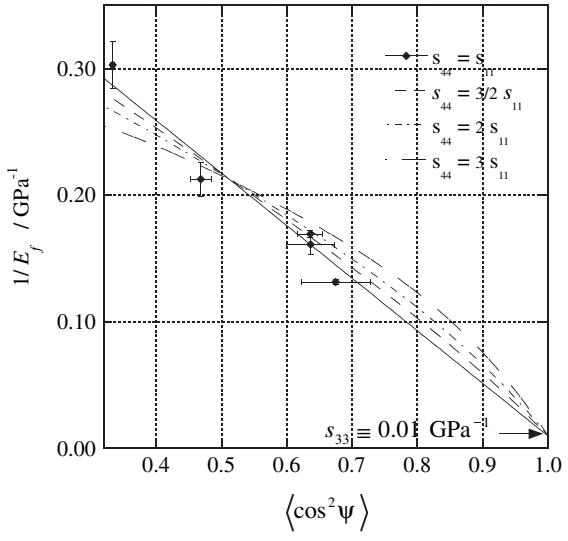

Fig. 5. An analysis of the orientation dependence of the fibre moduli in the context of the aggregate model. The fits to the experimental data correspond to the least-squares regression of Equation 12 assuming the stated relationships between the subunit shear and transverse compliances.

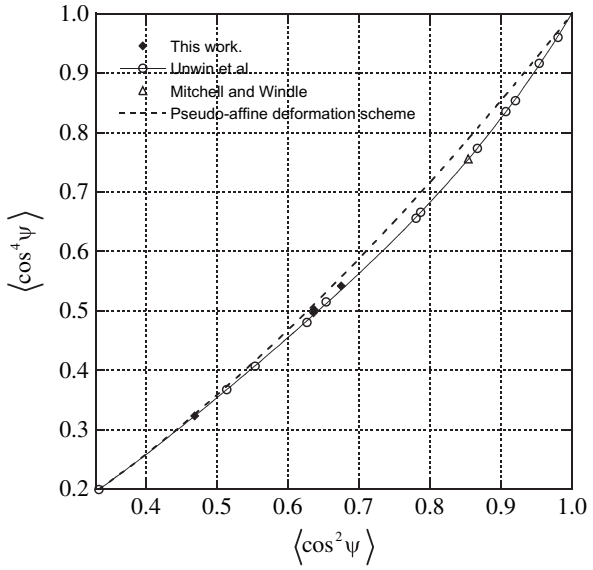

Fig. 6. The plot illustrates a generic relationship between the orientation averages $\langle\cos^2\psi\rangle$ and $\langle\cos^4\psi\rangle$ for uniaxially oriented polymers.

$$\left\langle\cos^4\psi\right\rangle = a + b\left\langle\cos^2\psi\right\rangle + c\left\langle\cos^2\psi\right\rangle^2 + d\left\langle\cos^2\psi\right\rangle^3 + e\left\langle\cos^2\psi\right\rangle^4, \tag{14}$$

for which the coefficients take values $a = 0.07$, $b = -0.368$, $c = 3.364$, $d = -3.911$ and $e = 1.845$. The relationship predicted by the pseudo-affine deformation scheme is also presented in the figure for comparison with the experimental data.

Given the following,

$$\left\langle\sin^2\psi\cos^2\psi\right\rangle = \left\langle\cos^2\psi\right\rangle - \left\langle\cos^4\psi\right\rangle, \tag{15}$$

the generic relationship between $\langle\cos^2\psi\rangle$ and $\langle\cos^4\psi\rangle$ could then be introduced into Equation 12. This analysis permitted additional fits to the experimental data assuming $s_{44} = 3/2\ s_{11}$, $s_{44} = 2\ s_{11}$ and $s_{44} = 3\ s_{11}$ the results of which are shown above in Fig. 5. It is seen that the quality of the fit provided by the aggregate model decreases as the ratio of the subunit shear and transverse compliances deviates from unity.

As a final test of the aggregate model the shear compliance of the aggregate has been evaluated assuming the equivalence of the subunit transverse and shear compliances using the following equation for an isotropic distribution of subunit orientations,

$$s'_{44} = \frac{14}{15}s_{11} - \frac{5}{15}s_{12} - \frac{8}{15}s_{13} + \frac{4}{15}s_{33} + \frac{2}{15}s_{44}. \tag{16}$$

Taking $s_{11} = s_{44} = 0.43 \pm 0.01$ GPa^{-1} and $s_{33} = 0.01$ GPa^{-1}, and appropriate values for the subunit Poisson's ratios [38], $\nu_{12} = 0.7$ and $\nu_{13} = 0.4$, the value predicted for the bulk isotopic shear modulus is, $G = 1/s'_{44} = 1.27 \pm 0.05$ GPa. This is in good agreement with the result obtained from dynamic torsional measurements performed on an unoriented bar of 75-AD material given in Table 4.

5. Conclusions

A mechanical and structural study of the properties of novel thermotropic copolyesters developed by Smith & Nephew® for potential applications in orthopaedic medicine has been presented in this work. The materials, derived from the random synthesis of *p*-hydroxybenzoic acid, vanillic acid, 4,4′-sulfonyl *bis*

(2-methylphenol) (dBPS) and each of adipic acid, suberic acid and azelaic acid, were successfully processed via melt-spinning to produce oriented fibres.

WAXD studies have demonstrated that the polymer chains possess nematic order, however, efficient lateral chain packing is clearly frustrated – presumably due to the intrinsic chemical disorder associated with the polymer composition.

A generic analysis of the material elastic properties has also been presented in the context of the aggregate model to obtain an understanding of the development of mechanical anisotropy with increasing molecular orientation. From the analysis of the fibre tensile moduli it is concluded transverse and shear compliances of the aggregate subunit – on which the bulk material properties are modeled – are equivalent, $s_{44} = s_{11} = 0.43 \pm 0.01$ GPa^{-1}. This result predicts a bulk isotropic shear modulus, $1/s'_{44} = 1.27 \pm 0.05$ GPa, which is in good agreement the experimental measurement, $G = 1.2 \pm 0.1$ GPa. In conclusion the aggregate model is considered to provide a suitable framework in which the development of mechanical anisotropy within these materials can be readily understood.

The low levels of molecular orientation achieved in this study, as evidenced by the low values for the order parameters determined from fibre WAXD patterns, are reflected in the comparatively low fibre tensile moduli, typically 5–7 GPa. In this regard further developments are necessary to address the mechanical requirements for high-load bearing orthopaedic applications as initially envisaged.

Acknowledgements

The authors wish to thank Prof. J.W. Goodby, Dr. I.M. Saez and Dr. A.D. Wilson within the Liquid Crystals Group at the University of York for their work on the synthesis of the materials studied in this work. This project received funding from Yorkshire Forward (Yorkshire & Humber Regional Development Agency). Project part financed by the European Union European Regional Development Fund. C.S. Lovell would like to thank the EPSRC and Smith & Nephew® for their sponsorship through an EPSRC CASE Award.

Appendix A. Evaluation of orientation averages and order parameters

Orientation averages were evaluated from the azimuthal dependence of the fibre equatorial intensity, $I(\alpha_i)$, using

$$\left\langle \cos^2\alpha \right\rangle = \frac{\sum_i I(\alpha_i)\sin\alpha_i \cos^2\alpha_i}{\sum_i I(\alpha_i)\sin\alpha_i} \tag{A.1}$$

and

$$\left\langle \cos^4\alpha \right\rangle = \frac{\sum_i I(\alpha_i)\sin\alpha_i \cos^4\alpha_i}{\sum_i I(\alpha_i)\sin\alpha_i}. \tag{A.2}$$

Additional relationships applied in calculating order parameters from results given by the above, and Equations (3)–(6) in the main text, were:

$$\left\langle \cos^2\psi \right\rangle = \frac{1}{3}(\langle P_0(\cos\psi)\rangle + 2\langle P_2(\cos\psi)\rangle) \tag{A.3}$$

and

$$\left\langle \cos^4\psi \right\rangle = \frac{1}{35}(7\langle P_0(\cos\psi)\rangle + 20\langle P_2(\cos\psi)\rangle + 8\langle P_4(\cos\psi)\rangle). \tag{A.4}$$

Finally, in addition to Equation 15 in the main text the following relationships were applied in the aggregate model analysis to derive Equation 12 from Equation (9):

$$\left\langle \sin^2\psi \right\rangle = 1 - \left\langle \cos^2\psi \right\rangle, \tag{A.5}$$

and

$$\left\langle \sin^4\psi \right\rangle = \left\langle \sin^2\psi \right\rangle - \left\langle \sin^2\psi \cos^2\psi \right\rangle. \tag{A.6}$$

References

[1] Ratner B, Hoffmann A, Schoen F, Lemmons J, editors. Biomaterials science: an introduction to materials in medicine. San Diego: Academic Press; 1996.
[2] Middleton JC, Tipton AJ. Synthetic biodegradable polymers as orthopedic devices. Biomaterials 2000;21(23):2335–46.
[3] Montes de Oca H, Ward IM, Klein PG, Ries ME, Rose J, Farrar D. Solid state nuclear magnetic resonance study of highly oriented poly(glycolic acid). Polymer 2004;45(21):7261–72.
[4] Montes de Oca H. Production and properties of oriented bioresorbable poly (glycolic acid) fibres. Phd: University of Leeds; 2005.
[5] Montes de Oca H, Ward IM. Structure and mechanical properties of pga crystals and fibres. Polymer 2006;47:7070–7.
[6] Montes de Oca H, Ward IM. Structure and mechanical properties of poly (l-lactic acid) crystals and fibers. Journal of Polymer Science, Part B: Polymer Physics 2007;45:892–902.
[7] Gomes ME, Reis RL. Biodegradable polymers and composites in biomedical applications: from catgut to tissue engineering – part 1-available systems and their properties. International Materials Reviews 2004;49(5):261–73.
[8] Kricheldorf HR, Stukenbrock T. New polymer syntheses .92. biodegradable, thermotropic copolyesters derived from beta-(4-hydroxyphenyl)propionic acid. Macromolecular Chemistry and Physics 1997;198(11):3753–67.
[9] Haderlein G, Schmidt C, Wendorff JH, Greiner A. Synthesis of hydrolytically degradable aromatic polyesters with lactide moieties. Polymers for Advanced Technologies 1997;8(9):568–73.
[10] Haderlein G, Petersen H, Schmidt C, Wendorff JH, Schaper A, Jones DB, et al. Synthesis and properties of liquid crystalline aromatic copolyesters with lactide moieties. Macromolecular Chemistry and Physics 1999;200(9):2080–7.
[11] Nagata M. Synthesis, characterisation, and hydrolytic degradation of copolyesters of 3-(4-hydroxyphenyl) propionic acid and p-hydroxybenzoic acid, vanillic acid, or syringic acid. Journal of Applied Polymer Science 2000;78: 2474–81.
[12] Nagata M, Nakae M. Synthesis, characterization, and in vitro degradation of thermotropic polyesters and copolyesters based on terephthalic acid, 3-(4-hydroxyphenyl)propionic acid, and glycols. Journal of Polymer Science, Part A: Polymer Chemistry 2001;39(18):3043–51.
[13] Chen YW, Wombacher R, Wendorff JH, Greiner A. Thermotropic aromatic/lactide copolyesters with solubilizing side chains on aromatic rings. Polymer 2003;44(19):5513–20.
[14] Chen YW, Jia ZH, Schaper A, Kristiansen M, Smith P, Wombacher R, et al. Hydrolytic and enzymatic degradation of liquid-crystalline aromatic/aliphatic copolyesters. Biomacromolecules 2004;5(1):11–6.
[15] Choy C. Elastic moduli of polymer liquid crystals. In: Brostow W, editor. Mechanical and thermophysical properties of polymer liquid crystals. London: Chapman & Hall; 1998. p. 448–94.
[16] Ward IM, Sweeney J. An introduction to the mechanical properties of solid polymers. 2nd ed. Chichester: John Wiley & Sons, Inc; 2004.
[17] Wang XJ, Zhou QF. Liquid crystalline polymers. Singapore: World Scientific Publishing; 2004.
[18] Montes de Oca H, Dagger A, Penrose A, Langton D, Anderson M, Farrar D, et al. Liquid crystalline bioresorbable polymers for use in orthopaedics, in preparation.
[19] Donald AM, Windle AH. Liquid crystalline polymers. In: Cambridge solid state science series. 2nd ed. Cambridge: Cambridge University Press; 1992.
[20] Franck A. Evaluation of the correct modulus in rectangular torsion. Tech. Rep.; TA Instruments.
[21] Duckett RA. Anisotropic yield behaviour. In: Ward IM, editor. Structure and properties of oriented polymers. 2nd ed. London: Chapman & Hall; 1997. p. 377–422.
[22] Blumstein A, Lin C, Mithal A, Tayebi A. Fibers from flexible liquid crystal main-chain polymers. 1. polymers based on 4,4′-dihydroxy-2,2′-dimethylazoxybenzene and alkyl dicarboxylic acids and alkyl dihalides. Journal of Applied Polymer Science 1990;41:995–1007.
[23] Blackwell J, Gutierrez G. The structure of liquid-crystalline copolyester fibers prepared from para-hydroxybenzoic acid, 2,6-dihydroxy naphthalene, and terephthalic acid. Polymer 1982;23(5):671–5.
[24] Blackwell J, Biswas A, Bonart RC. X-ray studies of the structure of liquid-crystalline copolyesters–treatment of an atomic model as a one-dimensional paracrystal. Macromolecules 1985;18(11):2126–30.
[25] Biswas A, Blackwell J. X-ray-diffraction from liquid-crystalline copolyesters–matrix-methods for intensity calculations using a one-dimensional paracrystalline model. Macromolecules 1987;20(12):2997–3002.

[26] Biswas A, Blackwell J. 3-Dimensional structure of main-chain liquid-crystalline copolymers .1. Cylindrically averaged intensity transforms of single chains. Macromolecules 1988;21(11):3146–52.
[27] Green DI, Collins TLD, Davies GR, Ward IM. Structure and mechanical properties of a thermotropic liquid crystalline copolyester. Polymer 1997;38 (21):5355–61.
[28] Mitchell GR, Windle AH. Conformational-analysis of oriented non-crystalline polymers using wide angle x-ray-scattering. Colloid and Polymer Science 1982;260(8):754–61.
[29] Mitchell GR, Windle AH. Measurement of molecular-orientation in thermotropic liquid-crystalline polymers. Polymer 1983;24(12):1513–20.
[30] Mitchell GR, Windle AH. Orientation in liquid crystalline polymers. In: Basset D, editor. Developments in crystalline polymers, vol. 2. London: Elsevier Applied Science; 1988. p. 115–75.
[31] Deas HD. The diffraction of x-rays by a random assemblage of molecules having partial alignment. Acta Crystallographica 1952;5(4):542–6.
[32] Bower D. Orientation distribution functions for uniaxially oriented polymers. Journal of Polymer Science, Part B: Polymer Physics 1981;19:83–107.
[33] Ward IM. Optical and mechanical anisotropy in crystalline polymers. Proceedings of the Physical Society of London 1962;80(517):1176–88.
[34] Troughton MJ, Davies GR, Ward IM. Dynamic mechanical-properties of random copolyesters of 4-hydroxybenzoic acid and 2-hydroxy 6-naphthoic acid. Polymer 1989;30(1):58–62.
[35] Green DI, Unwin AP, Davies GR, Ward IM. An aggregate model for random liquid-crystalline copolyesters. Polymer 1990;31(4):579–85.
[36] Zhang H, Davies GR, Ward IM. Mechanical-properties of thermotropic liquid-crystalline polyesters and polyamides. Polymer 1992;33(13):2651–8.
[37] Unwin AP, Bower D, Ward I. The determination of molecular orientation in oriented polypropylene by wide angle x-ray diffraction, polarized fluorescence and refractive index measurements. Polymer 1985;26:1605–10.
[38] Sweeney J, Brew B, Duckett RA, Ward IM. Mechanical anisotropy and inhomogeneity of an aromatic liquid-crystalline polyester. Polymer 1992;33(23):4901–7.